

## ANALYSIS OF A VERTICAL SEGMENTAL SHAFT USING 2D & 3D FINITE ELEMENT CODES

\* Vasiliki N. Georgiannou<sup>1</sup>, Andreas Serafis<sup>2</sup> and Eleni-Maria Pavlopoulou<sup>3</sup>

<sup>1,2,3</sup> National Technical University of Athens, Greece

\*Corresponding Author, Received: 23 Dec. 2016, Revised: 01 Feb. 2017, Accepted: 24 Feb. 2017

**ABSTRACT:** This computational research investigates the method of supporting underground cylindrical openings using prefabricated elements. The “Underpin” method is used to simulate the excavation and support of a vertical cylindrical shaft constructed in dry low cohesion soil layers. The primary objective of this study is to determine the stress distribution around the shaft due to three dimensional loading conditions. To this end the excavation is initially simulated as an axisymmetric problem using the “PLAXIS 2D” finite element program. The aforementioned method of analysis is subsequently verified against the equivalent “PLAXIS 3D” finite element analysis.

Attention has been directed towards recognising the crucial parameters affecting the analysis. It has been found that the constitutive model adopted to simulate the soil behavior (“Mohr-Coulomb” or “Hardening-Soil” model) is of paramount importance and that the shaft diameter also has some influence. However, variations of the shear strength parameters ( $c$ ,  $\phi$ ) at the soil-structure interface as well as in the value of “Unloading-Reloading Modulus” ( $E_{ur}$ ) have shown only a minor influence on the results of the analysis.

Floor uplift due to unloading, the development of an excessive plastic zone around the bottom of the vertical shaft, significant surface settlement around the shaft and most importantly the high values of tangential hoop stresses observed in the circular segmental rings, are the main issues raised in the calculations.

*Keywords: Cylindrical shaft, Underpin method, Numerical analysis, Stresses, Deformations*

### 1. INTRODUCTION

The excavation, support sequence and material properties used in the analysis simulate the construction of a 24m deep underground shaft, excavated and supported downwards, by a sequence described as the ‘underpin’ excavation and support method, in seventeen stages using prefabricated concrete elements (PCC segments). The PCC segments are placed at the base of the excavation as shown in Fig. 1, in soil layers with temporary self-supporting capability. The annulus between their outside perimeter and the excavated ground is immediately grouted with bentonite; not only to avoid soil disturbance but to transfer the segments’ gravity loads to the excavated vertical face of the shaft. This reduces the risk of overloading the upper rings which could pull down the whole ring build, due to lack of friction between the structure and the ground. A concrete collar may be constructed around the first segmental ring to provide a connection with the ground surface. Excavation of the next ring is commenced once the bentonite reaches its recommended strength. One segmental ring is installed and grouted at a time (i.e. corresponding to each simulation phase). The underpin segments are installed using a specialised handling / lifting frame. The use of prefabricated elements reduces

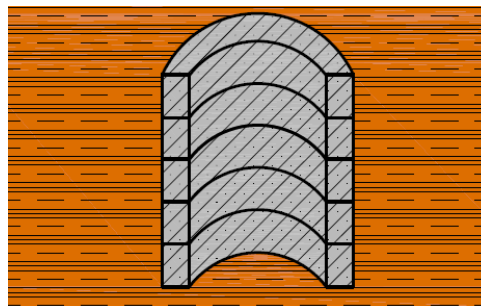


Fig.1 A perspective view of the “Underpin method”

costs due to reduced time of installation and at the same time improves safety and environmental impact because of the reduced size of the construction site (The British Tunnelling Society and the Institution of Civil Engineers, 2004 [1], Elnabolsy, 2015 [2], Aye et al., 2014 [3]).

The main advantage of the cylindrical underground openings is the global development of stresses along the shaft without any stress concentrations arising due to uniform lateral compressive loading. The excavation and installation of the segment leads to redistribution of the stresses in the ground. Figure 2 shows the stresses on a typical cross section of a cylindrical structure under uniform lateral compressive loading. Several attempts have been made to study

the lateral earth pressure distribution against cylindrical shafts in cohesionless media. Westergaard, 1940 [4] and Terzaghi, 1943 [5], proposed analytical solutions; Prater, 1977 [6] used the limit equilibrium method; and Berezantzev, 1958 [7], Cheng et al., 2007 [8], Liu and Wang, 2008 [9], Liu et al., 2009 [10] used the slip line method. In contrast to the classical earth pressure theories, where the active earth pressure calculated using the Coulomb, 1776 [11] or Rankine, 1857 [12] method are essentially the same, the distributions obtained for axisymmetric conditions may differ considerably depending on the chosen method of analysis. Kim et al., 2013 [13] conducted centrifuge model tests and full-scale field tests on vertical shafts and concluded that the lateral earth pressure acting on a circular vertical shaft is less than in other types of geotechnical structures due to three dimensional arching effects; as a result the magnitude and distribution of the lateral earth pressures is not linear with increasing excavation depth. This stress distribution results in reduced reinforcement compared to non-cylindrical shafts subjected to local stress concentrations (Muramatsu and Abe, 1996 [14], Dias et al., 2015 [15]). Benmebarek et al., 2013 [16], performed a numerical study to investigate the earth pressure distribution on a cylindrical shaft and also concluded that the axisymmetric active earth pressure distribution for cylindrical shafts does not increase linearly with depth as it does under plane strain conditions.

In this study the excavation and installation procedures during shaft construction in a 'soft soil' are simulated with the use of 2D and 3D finite element codes to identify:

- 1) the crucial parameters affecting the stresses and deformations developed around the shaft during construction;
- 2) the tangential (hoop) forces developed along the shaft;
- 3) the critical construction phase with respect to bottom uplift and maximum hoop forces developed over the segmental support;
- 4) the influence of the interface strength " $R_{inter}$ " (i.e. fully bonded wall ( $R_{inter}=1$ ) and  $R_{inter}=2/3$ ), and of plate connection type (i.e. rigid (clamped) plate connection c.f. hinge plate connection) on the bottom uplift, settlements and hoop forces,
- 5) the applicability of the 2D analysis for the 'Underpin' method by comparing the results of 3D analysis with those obtained from the 2D analysis.

Additionally, the factor of safety against the development of a failure mechanism within the soil around the shaft is computed using the " $\phi$ -c' reduction" procedure included in PLAXIS.

The purpose of this paper is twofold: first to determine the stress distribution and the deformation patterns around a cylindrical shaft,

based on the results of axisymmetric 2D finite element analyses, and second to verify the results against the equivalent 3D finite element analyses.

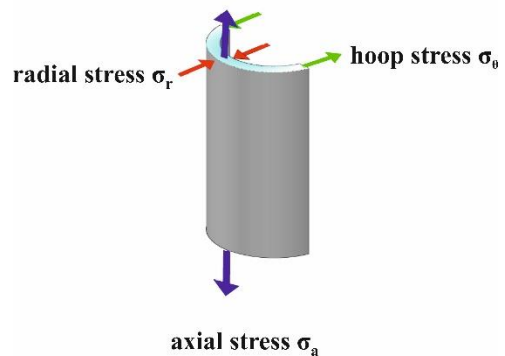


Fig.2 Stresses on a typical cross section of a cylindrical structure under uniform lateral compressive loading

## 2. NUMERICAL MODEL

The shaft under consideration is constructed in horizontal soil layers comprised of silty sands, at the top 17m, overlying sandy silts. The soil properties are included in Tables 1 and 2 respectively. A common final depth of excavation of 24m is used in the analyses while typical shaft diameters are adopted in the parametric study i.e. 10m and 16m. The parametric studies are performed under dry soil conditions. The "Mohr-Coulomb" and "Hardening Soil" models are used to simulate the soil behavior with the corresponding soil parameters included in Tables 1 and 2. Material properties at the interface between the segments and the soil are also included in the Tables. The segments are 30cm thick and 1.5m high. Details of the material properties of the segments are shown in Table 3. Each excavation stage includes the installation of a segment ring and a simultaneous excavation of 1.5m soil layer to be supported in the next stage. Finally, at last stage (stage 17) a 15cm deep lean concrete layer covers the bottom of the shaft.

## 3. RESULTS OF 2D NUMERICAL ANALYSES

The PLAXIS 2D finite element code was used initially to perform parametric analyses with varying shaft diameter, soil model, interface strength and plate connection type. Figure 3 shows the nodes chosen to represent bottom uplift and settlement. Node A is lying at the centre of the shaft bottom while the surface nodes B & C have been selected on the ground at 5m and 10m distance from the vertical face of the top segment respectively.

Table 1 Geotechnical parameters used in the ‘Mohr-Coulomb’ model

Parameter	Symbol	Silty Sand	Silty Sand “Custom interface”	Sandy Silt	Sandy Silt “Custom interface”
Material Model	Model	Mohr- Coulomb	Mohr- Coulomb	Mohr- Coulomb	Mohr- Coulomb
Drainage Type	Type	Drained	Drained	Drained	Drained
Unit weight above phreatic level	$\gamma_{\text{unsat}}$ (kN/m <sup>3</sup> )	16	16	17	17
Unit weight below phreatic level	$\gamma_{\text{sat}}$ (kN/m <sup>3</sup> )	20	20	20	20
Effective Young’s modulus	E’ (kN/m <sup>2</sup> )	7000	7000	6000	6000
Effective Poisson’s ratio	$\nu'$	0.3	0.3	0.3	0.3
Cohesion	c’ (kN/m <sup>2</sup> )	5	1	25	1
Friction angle	$\phi'$ (°)	30	30	24	24
Dilatancy angle	$\psi$ (°)	0	0	0	0
Interface reduction factor	R <sub>inter</sub>	0.7	1	0.5	1
Lateral earth pressure coefficient	K <sub>0</sub>	0.5	0.5	0.593	0.593

Table 2 Geotechnical parameters used in the ‘Hardening Soil’ model

Parameter	Symbol	Silty Sand (E <sub>ur</sub> =4*E <sub>50</sub> )	Sandy Silt (E <sub>ur</sub> =4*E <sub>50</sub> )
Material Model	Model	Hardening Soil	Hardening Soil
Drainage Type	Type	Drained	Drained
Unit weight above phreatic level	$\gamma_{\text{unsat}}$ (kN/m <sup>3</sup> )	16.0	17.0
Unit weight below phreatic level	$\gamma_{\text{sat}}$ (kN/m <sup>3</sup> )	20.0	20.0
Secant stiffness for CD triaxial test	E <sub>50</sub> <sup>ref</sup> (kN/m <sup>2</sup> )	14000	12000
Tangent oedometer stiffness	E <sub>oed</sub> <sup>ref</sup> (kN/m <sup>2</sup> )	7000	6000
Unloading /Reloading stiffness	E <sub>ur</sub> <sup>ref</sup> (kN/m <sup>2</sup> )	56000	48000
Power for stress level dependency of stiffness	m	0.5	0.5
Cohesion	c’ (kN/m <sup>2</sup> )	5	25
Friction angle	$\phi'$ (°)	30	24
Dilatancy angle	$\psi$ (°)	0	0
Poisson’s ratio	$\nu'_{\text{ur}}$	0.2	0.2
Reference stress for stiffness	P <sub>ref</sub> (kN/m <sup>2</sup> )	100	100
Stress ratio in normally consolidated state	K <sub>0</sub> <sup>nc</sup>	0.45	0.45
Interface reduction factor	R <sub>inter</sub>	0.7	0.5
Lateral earth pressure coefficient	K <sub>0</sub>	0.500	0.593

Table 3 Plate properties

Parameter	Symbol	Lining (C 40/50)	Lean concrete (C 16/20)
Material Model	Model	Linear Elastic	Linear Elastic
Drainage Type	Type	Non porous	Non porous
Unit weight	$\gamma$ (kN/m <sup>3</sup> )	25.0	25.0
Normal stiffness	E*A(kN/m)	10.5*10 <sup>6</sup>	4.125*10 <sup>6</sup>
Flexural Rigidity	E*I(kNm <sup>2</sup> /m)	78750	7734
Effective Poisson’s ratio	$\nu'$	0.2	0.2
K <sub>0</sub> determination	----	Automatic	Automatic
Concrete thickness	D(m)	0.3	0.15

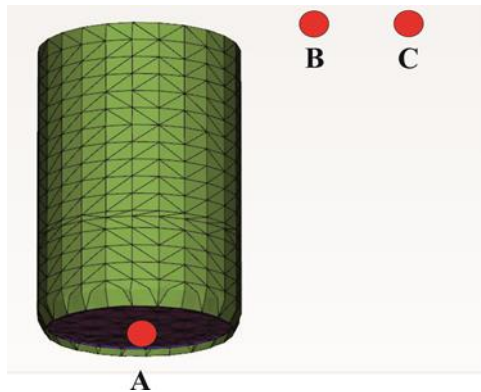


Fig.3 The three key-nodes used for monitoring bottom uplift and surface settlement

### 3.1 Critical Stage Of Analysis

The penultimate stage 16 is the critical stage of analysis due to: 1) the extended zone of ‘failure points’ concentrated at the unsupported periphery of the shaft bottom which results in the development of large displacements as shown in Figure 4 and 2) the development of the largest ‘hoop forces’ on the 16th segmental ring. In the ultimate stage 17 fewer “plastic points” develop and the additional displacements are negligible; similarly, the stress field components (M, Q, N, Hoop Forces) are negligible on the “final segmental ring” and “lean concrete”, since this stage in contrast to previous stages is not followed by another 1.5m deep excavation.

The minimum safety factor associated with the penultimate stage is calculated as 1.97 based on the “ $\phi$ -c’ reduction” method described in the “PLAXIS 2D ReferenceManual” [17], contrary to a safety factor of 4.5 associated with the ultimate stage of analysis. It should be noted that during the aforementioned calculations soil stiffness is not stress-dependent and hardening effects are not taken into account. Consequently, the stiffness is calculated at the beginning of each calculation phase and remains constant until the calculation phase is completed, irrespective of the soil model adopted in the analysis.

### 3.2 Floor Uplift – Failure Points

As observed in Figure 4, plastic points, where the stresses lie on the Mohr-Coulomb failure envelope, are concentrated at the periphery of the shaft bottom leading to local floor uplift. However, no plastic deformation is observed towards the central floor area indicating that the soil deforms as a solid body on unloading over this area. A detailed study of the local stress-strain curves, used to visualise the stress-strain behavior of the soil mass, further confirms that at the central floor area deformations are minimal and shear stresses are kept well below the shear strength of the soil. On

the contrary, the stress-strain curves for the plastic points located at the periphery, shown in Figure 5 for a typical point, indicate that failure conditions are reached. Finally, maximum floor uplift is shown to occur during the penultimate stage 16. The addition of lean concrete, in stage 17, marginally alleviates the uplift.

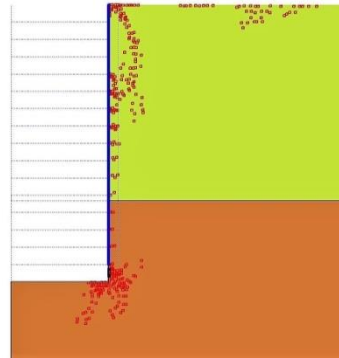


Fig.4 Plastic points around the excavation pit after Stage 16

### 3.3 Hoop Forces – A Detailed Description

Hoop forces reach values as high as 2.3 MN/m. Moreover, their magnitude varies non-uniformly with depth and reaches a peak towards the bottom end of the segmental ring. The observed non-uniformity can be explained by examining the construction stage sequence. In the process of removing a soil volume of 1.5m depth, the radial horizontal stresses,  $\sigma_{xx}$ , are removed. This is consequently accompanied by the development of horizontal strains,  $\epsilon_{xx}$ , on the self-supported soil vertical cut of 1.5m height. However, since the adopted construction sequence involves ring placement followed by excavation, during the next stage the placement of the segmental ring and the excavation of another 1.5m of soil below the ring results in a stress concentration arising on the bottom end of the ring due to the prevention of the development of incremental strains in the unsupported soil, hence the local increase of hoop stresses. Figure 6 depicts the horizontal stress concentration along the segments while Figure 7 plots the final tangential stress distribution after all segments are in place (Stage 17). It is observed that the largest hoop stresses develop in each segment on initial placement. Hoop forces increase with depth as a result of the increasing horizontal stresses. Finally, in stage 17 the last segmental ring and the lean concrete are placed, hence the former is free of any hoop forces in Figure 7.

Tobar and Meguid, 2010 [18], systematically evaluated a number of theoretical solutions predicting the earth pressure distribution on

cylindrical shafts constructed in sand. They found that for shallow shafts with a depth to diameter ratio lower than 2 all methods consistently predicted earth pressures close to active values. However, with increasing depth the predictions diverged as earth pressures significantly lower than the active values materialise. In the current study the depth to diameter ratio was 3 and the horizontal and tangential stresses decrease during excavation, the former to near zero values, and build up after the placement of the segments to values close to active pressures in agreement with the abovementioned observations. Koning et al., 1991 [19], modelled the unsupported area of the excavation in centrifuge tests as the shaft face advanced following the installation of the lining. They showed that for the stability of the excavation only a small support pressure was required. With regards to the lining, a stress concentration was observed close to the face of the excavation, which is reminiscent of the stress concentration shown in Figures 6 and 7.

### 3.4 Parametric Analysis

The soil model, the shaft diameter, the interface strength and the type of plate connection are shown to significantly affect the results. The

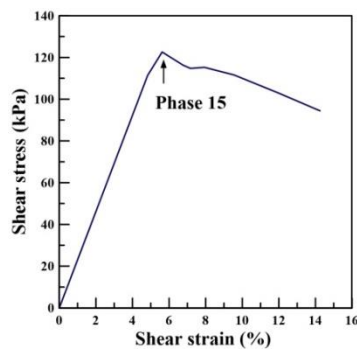


Fig.5 Stress point shear failure after stage 15

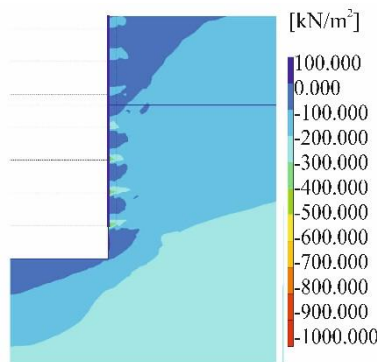


Fig.6 Horizontal stress concentration along segments; stage 16

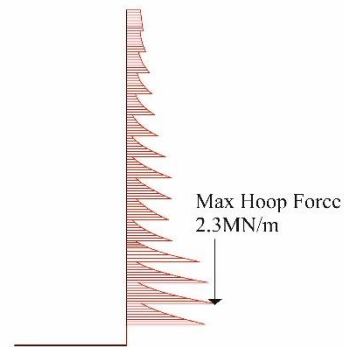


Fig.7 Distribution of 'hoop forces' along segments; stage 17

effect of the above parameters is examined next.

Regarding the soil model, it is observed that floor uplift is significantly larger when the Mohr-Coulomb model describes the soil behavior compared to the Hardening Soil model. This is attributed to the higher soil stiffness on unloading provided by the latter compared to the same soil stiffness irrespective of loading direction assumed by the former. On the other hand the larger the volume of excavated soil the higher the unloading and the uplift, hence, a change in the shaft diameter affects the uplift to a different degree depending on the soil model. As indicated in Figure 8 an increase in diameter from 10m to 16m results in a 30cm increase in uplift if the Mohr-Coulomb soil model is adopted compared to only 4cm for the Hardening Soil model. The results are also sensitive to the values of stiffness used. For relatively 'soft soils' such as the silty sands and sandy silts used in the analysis the stiffness on unloading/reloading is usually assumed as  $E_{ur}=4 \times E_{50}$ . As is evident from Figures 8(b) and (c), an increase in stiffness from 3 to  $4 \times E_{50}$  resulted in a 3 cm decrease in uplift for the 16m diameter shaft case. The decrease observed is approximately 25% for both diameters.

If the surface settlement curves are considered at a radial distance 5m and 10m (Figure 3) from the vertical face of the shaft while the Hardening Soil model is employed, a continuously increasing settlement is observed at the surface with subsequent stages of excavation and support; only in the initial stages the step displacement curves show uplift. However, neither the shaft diameter nor the aforementioned variation in the values of the unloading/reloading stiffness appears to affect the final settlement values in Figure 9. Surface settlement reaches final values of 2cm and 1cm at 5m and 10m away from the shaft respectively.

Assuming same stiffness on loading and unloading conditions, as in the Mohr-Coulomb soil

model, gives erroneous final results for surface settlement at the end of both 2D and 3D analyses. A 2cm uplift is obtained at the point 10m away from a 10m diameter shaft. To account for such discrepancies when applying the Mohr-Coulomb model the Poisson's ratio should be increased and the soil layers should be subdivided into layers of increasing stiffness to simulate stiffness increasing with depth as in the Hardening Soil model.

The shaft diameter significantly affects the 'hoop forces' when the 'Hardening Soil model' is applied while the effect of stiffness on unloading/reloading is insignificant as shown in Figure 10, indicating that hoop stresses are a direct result of the uniform lateral compressive stresses acting on the segment as it resists soil movement.

To simulate soil-structure interaction the interface strength parameter " $R_{inter}$ " (Vermeer P. Plaxis Bulletin, 2008) [20] is introduced, which allows for there to be a relative displacement between soil and segmental rings, and soil disturbance around the excavation. The parameter,  $R_{inter}$ , varies the soil strength parameters  $c'$  and  $\phi'$  at the interface depending on the bonding between soil and structure i.e. for a full roughness wall  $R_{inter}=1$ . Figure 11 shows the influence of the soil strength parameters at the interface on hoop forces

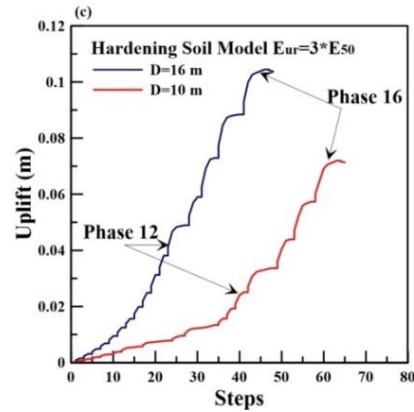
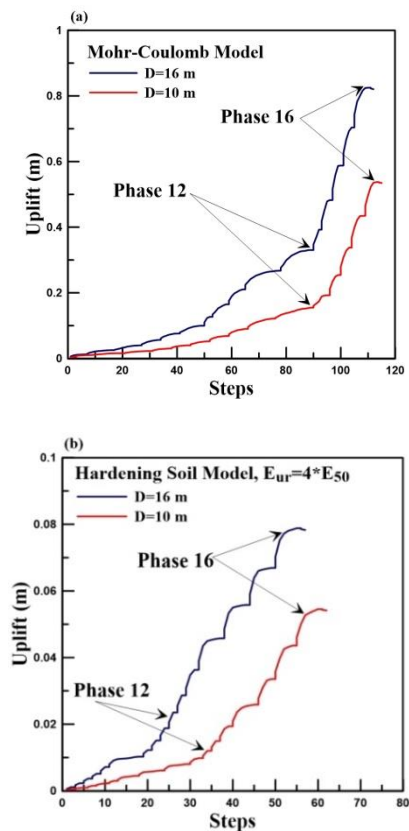
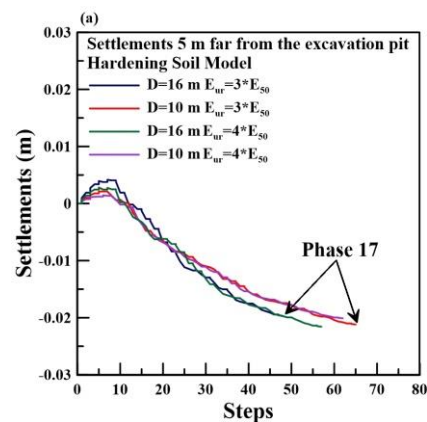


Fig. 8 Floor uplift; combined effect of soil model and shaft diameter: (a) Mohr-Coulomb; (b) & (c) Hardening Soil model; effect of soil stiffness on unloading

and surface settlements. The former decrease with soil disturbance ( $R_{inter}<1$ ) while the latter are not affected by the strength parameters adopted at the interfaces.

Finally, a hinge is a plate connection that allows for a discontinuous rotation about the point of connection (joint). By default, according to PLAXIS 2D, in a geometry point where plate ends come together, the rotation is continuous and the point contains only one rotational degree of freedom. In other words, the default plate connection is rigid (clamped). In Figure 12(a) it is evident that the hoop forces increase significantly when a hinge plate connection is introduced. The location of the largest hoop stresses is the same as observed previously in Figure 7. Correspondingly, bending moments show a dramatic drop in Figure 12(b); however, their values remain relatively low even in the case of a rigid connection.



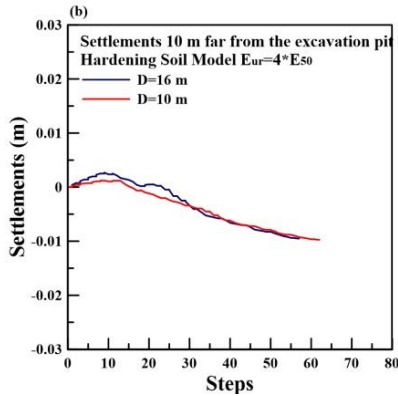


Fig. 9 Surface settlement; combined effect of soil stiffness on unloading and shaft diameter (a) 5m & (b) 10m away from the shaft

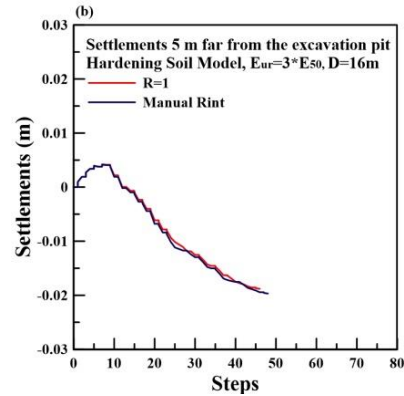


Fig. 11 The effect of soil strength at the interface on (a) Hoop forces; (b) Surface settlement

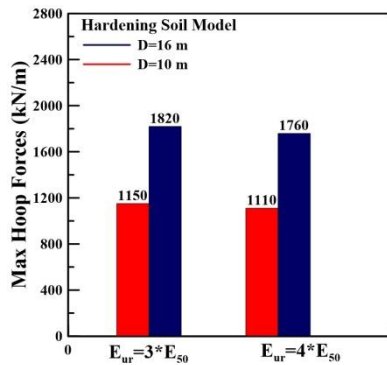


Fig. 10 Hoop forces; combined effect of soil stiffness on unloading and shaft diameter

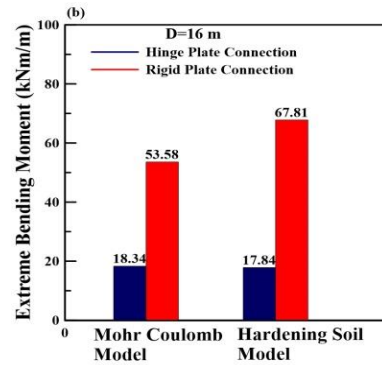
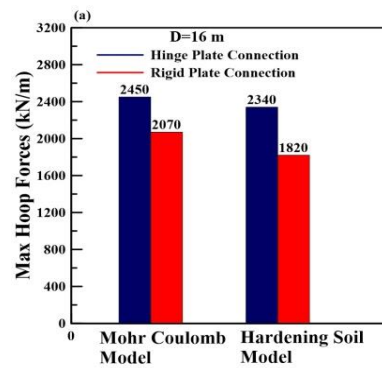
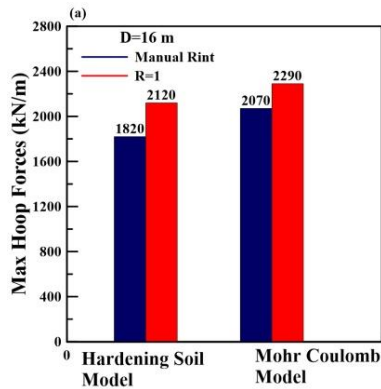


Fig. 12 The effect of plate connection type on (a) Hoop forces; (b) Bending moments



#### 4. PLAXIS 3D: COMPARATIVE RESULTS

The results of 3D analyses are used to assess the results of the 2D analyses described earlier. Table 4 includes the parameters adopted in each analysis i.e. shaft diameter, soil model, stiffness on unloading/reloading and interface strength, which were found to significantly affect the results of 2D analyses. The objective is to compare the results of 2D with 3D analysis using the same input variables. Comparison of floor uplift is made in Figure 13(a). In general similar values are

obtained for uplift with slightly higher values observed in the 2D analysis. The same degree of similarity is observed in Figure 13(b) where the maximum hoop forces are depicted. As previously observed in Figure 7 maximum hoop forces develop on the deep segmental rings.

Similar results are obtained with respect to horizontal stress concentration along segments i.e. by comparing Figures 6 (2D, D=16m) and 14 (3D, D=10m).

It appears that for the geotechnical application examined it is adequate to use a two dimensional analysis considering how time consuming the 3D analysis would be. Although the bottom of the shaft acts as a boundary that disrupts axisymmetry, the use of a 2D axisymmetric model yields comparable results with the 3D analysis at a much reduced time, allowing for a detailed parametric study to be performed.

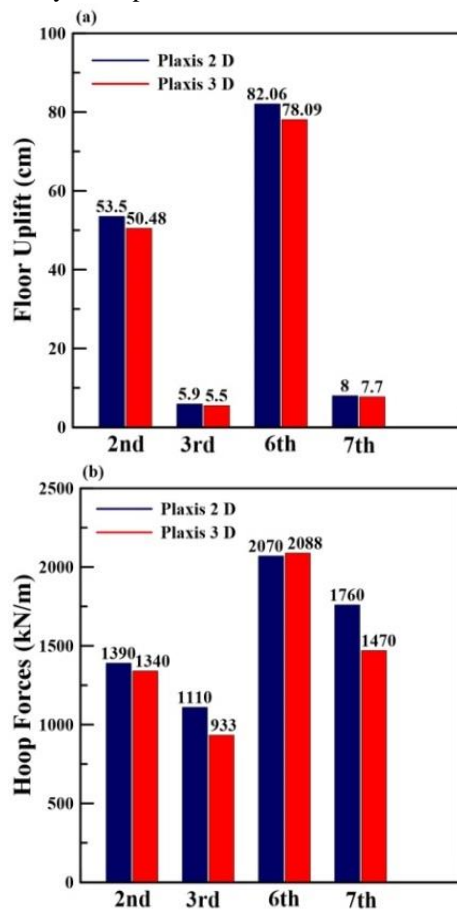


Fig. 13 2D vs 3D analysis: (a) Floor uplift; (b) Hoop forces

Table 4 Comparisons of 2D and 3D analyses

Shaft Diameter D(m)	Soil Model	Interface
1 <sup>st</sup> . 10	MC	1
2 <sup>nd</sup> . 10	MC	2
3 <sup>rd</sup> . 10	HSM, $E_{ur}^{ref} = 4 * E_{50}^{ref}$	2
4 <sup>th</sup> . 10	HSM, $E_{ur}^{ref} = 3 * E_{50}^{ref}$	2
5 <sup>th</sup> . 16	MC	1
6 <sup>th</sup> . 16	MC	2
7 <sup>th</sup> . 16	HSM, $E_{ur}^{ref} = 4 * E_{50}^{ref}$	2
8 <sup>th</sup> . 16	HSM, $E_{ur}^{ref} = 3 * E_{50}^{ref}$	2

Note: 1<sup>st</sup> to 8<sup>th</sup> analysis; MC: Mohr-Coulomb model, HSM: Hardening Soil model; 1: custom & 2: cluster material interface

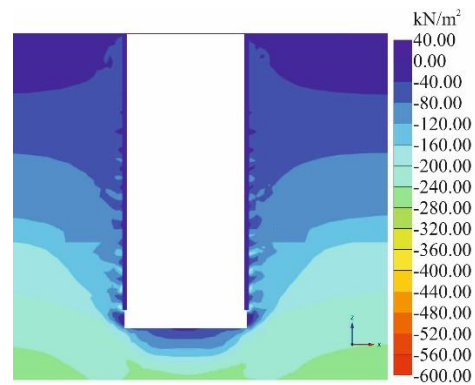


Fig. 14 Horizontal stress concentration along segments; 3D analysis of a 10m diameter shaft

## 5. CONCLUSION

The underpin method including staged excavation and segmental ring placement during shaft construction is simulated utilising PLAXIS 2D and 3D finite element programs.

Both programs indicate a hoop stress concentration at the bottom section of each segmental ring resulting in critically high values (2.3MN/m) only in this part of the ring's outer surface for the deepest segments.

Floor uplift can also be a matter of concern. To address this particular issue the Hardening Soil model, which takes into account soil stiffness variation with loading conditions, should be used in any analysis. Depending on stiffness on unloading floor uplift remained less than 10cm. Apart from the soil model the most influential parameter affecting uplift is the shaft diameter.

For this application and generally cylindrical shafts of equal or greater depth the axisymmetric 2D analysis gives similar results to the 3D analysis.

## 6. REFERENCES

- [1] The British Tunnelling Society and the Institution of Civil Engineers, "Tunnel lining design guide", Thomas Telford, London, UK, 2004, pp. 83-86.
- [2] Elnabolsy K., "Shaft Construction Methods Comparison", North American Society for Trenchless Technology, No-Dig Show, Denver, Colorado, 2015, MM-T4-01, pp. 1-16
- [3] Aye T.T., Tong M.S.Y., Yi K.H., Arunatoruban E., "Design and Construction of Large Diameter Circular Shafts". In: Underground Singapore, Singapore, 2014
- [4] Westergaard H.M., "Plastic state of stress around deep well", Boston Society of Civil Engineers Journal, Vol. 27, No.1, 1940, pp. 1-5.
- [5] Terzaghi K., "Theoretical soil mechanics", Wiley, New York, 1943.
- [6] Prater E.G., "Examination of some theories of earth pressure on shaft linings", Can. Geotech. J, 1977, 14(1), pp. 91-106.
- [7] Berezantzev V.G., "Earth pressure on the cylindrical retaining walls". In: Conference on Earth Pressure Problems, Brussels, 1958, pp. 21-27.
- [8] Cheng Y.M., Hu Y.Y., Wei W.B., "General axisymmetric active earth pressure by method of characteristics – theory and numerical formulation", *int. J. Geomech.* 2007; 7 (1) pp. 1-15.
- [9] Liu F.Q., Wang J.H., "A generalized slip line solution to the active earth pressure on circular retaining walls", *Comput. Geotech.* 2008; 35 (2) pp. 155-164.
- [10] Liu F.Q., Wang J.H., Zhang L.L., "Axisymmetric active earth pressure obtained by the slip line method with a general tangential stress coefficient", *Comput. Geotech.*, 2009, 36 (1-2), pp. 352-358
- [11] Coulomb C.A., "Essai sur une Application des Regles des Maximis et Minimis a Quelques Problemes de Statique Relatifs, a la Architecture", *Mem. Acad. Roy. Div. Sav*, Vol. 7, 1776, pp. 343-387
- [12] Rankine W.J.M., "On the stability of loose earth", *Philos. Trans. Roy. Soc. London*, 1857, vol. 147, pp. 9-27.
- [13] Kim K.Y., Lee D.S., Cho J.Y., Jeong S.S., "The effect of arching pressure on a vertical circular shaft", *Tunn. Undergr. Space Technol.* 37, 2013, pp. 10-21
- [14] Muramatsu M., Abe Y., "Considerations in shaft excavation and peripheral ground deformation". *International Symposium on Geotechnical Aspects of Underground Construction in soft ground*, London, 1996, pp. 173-178
- [15] Dias T.G.S., Farias M.M., Assis A.P., "Large diameter shafts for underground infrastructure", *Tunnelling and Underground Space Technology*, 2015, pp. 181-189
- [16] Benmebarek S., Meftah A. and Benmebarek N., "Numerical Study of the Earth Pressure Distribution on Cylindrical Shafts", *International Symposium on Innovative Technologies in Engineering and Science, Sakarya University Congress and Culture center*, 2013, pp. 283-292
- [17] PLAXIS Version 8, Reference Manual
- [18] Tobar T., Meguid M.A., "Comparative evaluation of methods to determine the earth pressure distribution on cylindrical shafts", *Tunnelling and Underground Space Technology*, 2009, pp. 188-197
- [19] Konig, D., Guettler, U., Jessberger, H.L., "Stress redistributions during tunnel and shaft constructions". In: *Proceedings of the International Conference Centrifuge*, Boulder, Colorado, 1991, pp. 129-135
- [20] Vermeer, P.A., *Plaxis Bulletin*, Column Vermeer, March 2008, pp. 5-8